Nonspreading Solutions in An Integro-Difference Model Incorporating Allee and Overcompensation Effects.

Garrett Otto *
Department of Mathematics
University of Louisville
Louisville, KY 40292

Bingtuan Li *
Department of Mathematics
University of Louisville
Louisville, KY 40292

*This research was partially supported by the National Science Foundation under Grant DMS-1515875

Abstract

Previous works in integro-difference models have generally considered Allee effects and overcompensation separately, and have focused on constant spreading speeds. Recent results obtained by Sullivan et al. (Proc. Natl. Acad. Sci. (2017) 114: 5053-5058) have shown that a combination of an Allee effect and overcompensation generates fluctuating spreading speeds. In this paper, we analytically prove that for a piecewise constant growth function exhibiting both an Allee effect and overcompensation, there exist equilibrium solutions vanishing at $\pm\infty$ across solid regions of parameter space. We numerically demonstrate that perturbations of the equilibrium solutions lead to solutions with various spatial patterns persisting essentially in compact domains. We also provide simulations to show that for growth functions involving the Ricker and Hill functions, stable equilibrium solutions with different periods exist, and patch formation can be developed.

Key words. Integro-difference equation, Allee effect, Overcompensation, Nonspreading solution.
AMS subject classification. 92D40, 92D25
Abbreviated title. Nonspreading Solutions in Integro-Difference Equation.

1 Introduction

One approach to modeling dispersal and reproduction makes use of integro-difference equations of the form

$$u_{n+1}(x) \;=\; Q[u_n](x) \;:=\; \big(k * g(u_n)\big)(x) \;=\; \int_{-\infty}^{\infty} k(x-y)\, g\big(u_n(y)\big)\, \mathrm{d}y. \tag{1}$$

where $u_n(x)$ is the density of individuals at point x and time n, $g(u)$ describes density dependent fecundity, and $k(x-y)$ is the dispersal function, which depends upon the distance $|y-x|$ between the location of birth y and the location of settlement x. Here individuals first undergo reproduction and then redistribute their offspring according to the dispersal function before reproduction occurs once again as in the case with annual plants and many insect species. The dispersal kernel in (1) is flexible. The shape of the dispersal kernel can be fitted to data from mark-recapture experiments and include rare, long-distance dispersal events observed with invasive spread [24, 46, 48, 51]. Integro-difference models have been used to predict changes in gene frequency [29, 30, 31, 47, 54], and applied to ecological problems [14, 15, 16, 17, 22, 23, 27, 21, 35].

An Allee effect arises when the per-capita birth rate increases with population density to some maximum value, although this effect usually disappears as increased intraspecific competition occurs. Models incorporating Allee effects have long been prominent in the ecological literature, dating back at least to Allee [1]. Allee effects may occur via various mechanisms [3, 2, 4, 6, 9, 10, 5, 12, 11, 13, 28, 34, 40, 49].

A spreading speed is the asymptotic speed at which a species initially introduced in a bounded domain expands its spatial range. Model (1) has a constant spreading speed that can be characterized as the slowest speed of a class of traveling waves, if $g(u)$ is monotone without a strong Allee effect and $g'(0) > 1$ (Weinberger [55]), or if g exhibits overcompensation without an Allee effect, $g'(0) > 1$, and $g(u) \le g'(0)u$ (Hsu and Zhao [18],Li et al. [26]). In the later case a traveling wave may have an oscillatory tail [26]. In the presence of a strong Allee effect, let α denote the Allee threshold. Assume that 0 and u^* with $u^* > \alpha$ are the other two equilibriua. Lui [31] proved that if g is nondecreasing and there is a strong Allee effect then model (1) has a constant spreading speed c which represents the only traveling wave speed. Wang et al. [53] showed that under appropriate conditions, c is positive, zero, or negative, if $\int_0^{u^*}[g(u)-u]du > 0$, $= 0$, or < 0, respectively. Note that the existence of solutions with zero spreading speed depends upon the critical condition $\int_0^{u^*}[g(u)-u]du = 0$, and is not robust in the sense that a slight change of model parameters can result in a solution with nonzero spreading speed.

In contrast to classic approaches that emphasize a constant spreading speed, there is growing empirical recognition that invasion dynamics can be highly variable and idiosyncratic [32, 37, 58, 59, 8, 52, 19]. There are several theoretical explanations for fluctuations in spreading speed, including stochasticity in either demography or dispersal [52, 19, 39, 25, 44] and temporal or spatial environmental heterogeneity [45, 36, 56, 57, 7, 43]. Recently Sullivan et al. [50] discovered that model (1) where $g(u)$ exhibits both an Allee effect and overcompensation can generate fluctuations in spreading speeds. The authors demonstrated that the fluctuations are induced by the combination of a strong Allee effect, which produces a pushed wave, and strong overcompensation, which produces large spatiotemporal variation in density behind the invasion front and thus, variation in the strength of the push, leading to fluctuating invasion speeds. The speed fluctuations can be periodic or more complex. The results highlight a new source of variability in biological invasions.

In this paper we study the spatial dynamics of (1) in a different direction. We show that a combination of an Allee effect and overcompensatory growth can produce biologically meaningful robust nonspreading solutions. Roughly speaking, a nonspreading solution is a solution which virtually persists in a bounded domain for all generations without expanding its spatial range. Such a solution describes 'invasion pinning' that has been investigated for coupled ordinary differential systems in a discrete (patch) environment (see Keitt et al. [20] and references therein). It is surprising to note that simple scalar integro-difference equations designed as a model tool to investigate spatial spread of populations possess biologically meaningful solutions that actually do not spread in a homogeneous continuous environment. We show that it is possible to identify solid regions in the parameter space where the system has one or even multiple nonspreading solutions. One consequence of existence of nonspreading solutions concentrated on bounded domains is growth of a species in multiple 'patches' apart from each other in space.

This paper is organized as follows. In the next section, rigorous results regarding the existence of equilibrium solutions vanishing at $\pm\infty$, for the case that $g(u)$ is a piecewise constant function, are provided. Section 3 is about numerical simulations demonstrating existence of nonspreading solutions with various spatial patterns for several growth functions. Section 4 includes some concluding remarks and discussions. The rigorous proofs of the theorems are given in the Appendix.

2 Existence of equilibrium solutions vanishing at $\pm\infty$

For the purposes of this paper we will limit our attention to piecewise continuous symmetric dispersal kernels. To demonstrate the existence of nonspreading solutions when strong Allee effect and overcompensation are present, we first analytically demonstrate the existence of continuous equilibrium solutions vanishing at $\pm\infty$ for a particular class of parameterized growth functions.

In this section we will first give some preliminary definitions and then present a theorem for the existence of equilibria within our particular class of fecundity functions. The theorem gives algebraic conditions in terms of the cumulative distribution function of $k(x)$ as well as the parameters of the growth function. When these conditions are satisfied it guarantees the existence of equilibria that vanish at $\pm\infty$.

We define our growth function to be a 3-level piecewise constant function. By way of scaling, we may in generality assume that the Allee threshold occurs at $u = 1$. The growth function, pictured in Figure 1-(a), is then given by

$$g(u) := \begin{cases} 0, & 0 \le u \le 1 \\ n_2, & 1 < u < n_1 \\ n_0, & u \ge n_1 . \end{cases} \tag{2}$$

The growth function is thus determined by the 3 positive parameters, n_0, n_1, n_2. There is a strong Allee effect in g. To exhibit overcompensation and have the possibility of non-decaying solutions, the parameters must satisfy the inequalities $n_0 < n_1 < n_2$ and $1 < n_1, n_2$. Under these conditions, $g(u)$ generates as period-2 cycle if $n_0 > 1$, or extinction if $n_0 < 1$.

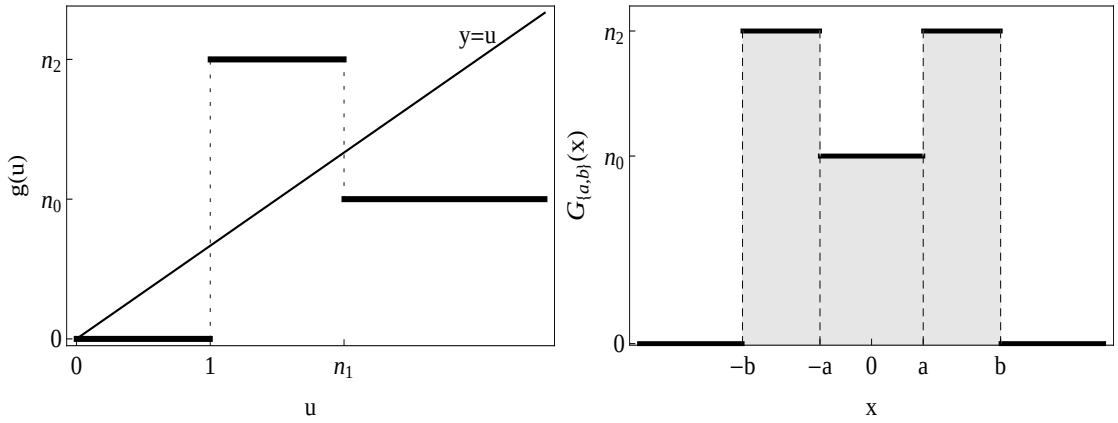

(a) Fecundity function and the line y=u.

(b) Plot of $G_{\{a,b\}}(x)$.

Figure 1: Plot of piecewise fecundity function, and $G_{\{a,b\}}(x)$.

To determine conditions for the existence of equilibria, we invoke the following ansatz about the form of the composition of the growth function with the equilibrium. For n_0, n_2 in (2) and $0 < a < b$, define

$$G_{\{a,b\}}(x) := \begin{cases} n_0, & |x| < a \\ n_2, & a < |x| < b \\ 0, & |x| > b . \end{cases} \tag{3}$$

The graph of $G_{\{a,b\}}$ is shown in Figure 1-(b). We seek an equilibrium solution, $u_e(x)$, of model (1) with $u_e(\pm\infty) = 0$ that satisfies

$$g(u_e(x)) = G_{\{a,b\}}(x) . \tag{4}$$

We see this form of $g(u_e(x))$ is consistent with u_e being a symmetric, uni-modal function where the following conditions hold:

Condition (C1)

1. $u_e(\pm a) = n_1$,
2. $u_e(\pm b) = 1$,
3. $u_e(0) > n_1$.

Invoking equation (4) we find $u_e(x) = \big(k * G_{\{a,b\}}\big)(x)$, and therefore Condition C1 implies

1. $\big(k * G_{\{a,b\}}\big)(a) = n_1$,
2. $\big(k * G_{\{a,b\}}\big)(b) = 1$,
3. $\big(k * G_{\{a,b\}}\big)(0) > n_1$.

Letting $K(x) = \int_{-\infty}^{x} k(s)\mathrm{d}s$, we define the following expressions

$$
\begin{aligned}
A(a,b) &:= \big(k * G_{\{a,b\}}\big)(a) - n_1 \\
&= -n_1 - \frac{(n_2+n_0)}{2} + n_2\Big(K(a+b) + K(b-a)\Big) - (n_2-n_0)K(2a)\ , \\
B(a,b) &:= \big(k * G_{\{a,b\}}\big)(b) - 1 \\
&= -1 + n_2\Big(K(2b) - \frac{1}{2}\Big) + (n_2-n_0)\Big(K(b-a) - K(b+a)\Big)\ , \\
C(a,b) &:= \big(k * G_{\{a,b\}}\big)(0) - n_1 \\
&= -(n_1+n_0) + 2n_2 K(b) - 2(n_2-n_0)K(a)\ .
\end{aligned}
\tag{5}
$$

We present the following theorem regarding the existence of equilibrium solutions.

Theorem 2.1. Assume there exists an a, b where $0 < a < b$ such that

$$A(a,b) = 0, \quad B(a,b) = 0, \quad C(a,b) > 0,$$

and $u_e(x) := \int k(x-y)\, G_{\{a,b\}}(y)\,\mathrm{d}y$ satisfies

$$u_e(x) > n_1 \text{ for } |x| < a, \quad 1 < u_e(x) < n_1 \text{ for } a < |x| < b, \quad \text{and } u_e(x) < 1 \text{ for } |x| > b.$$

Then $u_e(x)$ is an equilibrium solution of model (1).

The proof of Thm. 2.1 is presented in Appendix A. To determine further results the dispersal kernel must be specified. In the following sections we analyze the case of the uniform and Gaussian dispersal kernels. Clearly the equilibrium solutions given in this theorem become zero at $\pm\infty$.

2.1 Uniform dispersal kernel

We consider $k(x)$ to be the symmetric uniform distribution with support $(-\frac{1}{2}, \frac{1}{2})$,

$$k(x) = \begin{cases} 0, & |x| > \frac{1}{2} \\ 1, & |x| \le \frac{1}{2}. \end{cases}$$

By appropriate scaling this choice of kernel can represent any centered uniform distribution. While perhaps not totally biologically realistic, this may be considered the limiting case of several families of distributions, as they are made more platykurtic while fixing the variance. For instance, the exponential power distribution $\frac{\beta \exp\left(-\frac{|x|^\beta}{\alpha^\beta}\right)}{2\alpha\Gamma\left(\frac{1}{\beta}\right)}$ converges almost-everywhere to $U(-\frac{1}{2},\frac{1}{2})$ as $\beta \to \infty$ with $\alpha = \frac{1}{2}$.

We are able to give a simple characterization for when parameters n_0, n_1, n_2 have an associated equilibrium. We first define the following functions of n_0, n_1, n_2 :

$$\hat{a}(n_0,n_1,n_2) := \frac{2n_0(n_1-n_2)+n_2(2-2n_1+n_2)}{4(n_2-n_0)^2} \tag{6}$$

$$\hat{b}(n_0,n_1,n_2) := \frac{2n_0^2+n_2(6-2n_1+n_2)+2n_0(n_1-2n_2-2)}{4(n_2-n_0)^2}.$$

We also define $\mathscr{A}$ to be the open triangular region in the (a,b) plane with vertices $(0,\frac{1}{2})$, $(\frac{1}{4},\frac{3}{4})$, $(\frac{1}{4},\frac{1}{4})$. $\mathscr{A}$ is depicted in Figure 2.

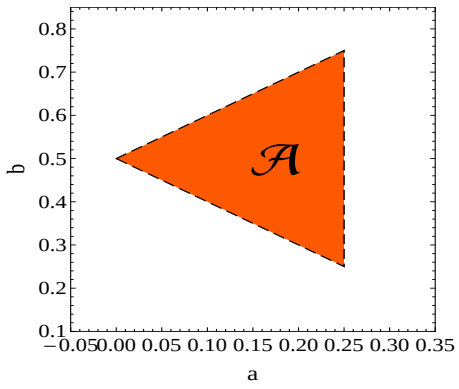

Figure 2: Region $\mathscr{A}$ of the (a,b) plane.

The following theorem then characterizes the equilibrium solutions.

Theorem 2.2. If $\left(\hat{a}(n_0,n_1,n_2), \hat{b}(n_0,n_1,n_2)\right) \in \mathscr{A}$ then there exists an equilibrium solution given by $u_e(x) = \left(k * G_{\left\{\hat{a}(n_0,n_1,n_2),\, \hat{b}(n_0,n_1,n_2)\right\}}\right)(x)$ for model (1).

The proof of theorem 2.2 is provided in Appendix B.

The equilibria are robust in the parameter space $\{(n_0,n_2,n_3) \in \mathbb{R}^3 | n_2 > n_1 > n_0;\ n_1,n_2 > 1, n_0 > 0\}$ in the sense that they exists on set of full-measure in the parameter space. To demonstrate this, in Figure 3 we show a region plot of where equilibria exist for constant n_2 slices of the parameter space.

A typical equilibrium is depicted in Figure 4. For the parameter values depicted $\hat{a} = 0.2275$ and $\hat{b} = 0.5775$. We see the function is a linear spline, as would be expected from the convolution of two piecewise constant functions. The support for u_e is of course compact, as would be expected since both k and $G_{\{\hat{a},\hat{b}\}}$ have compact support.

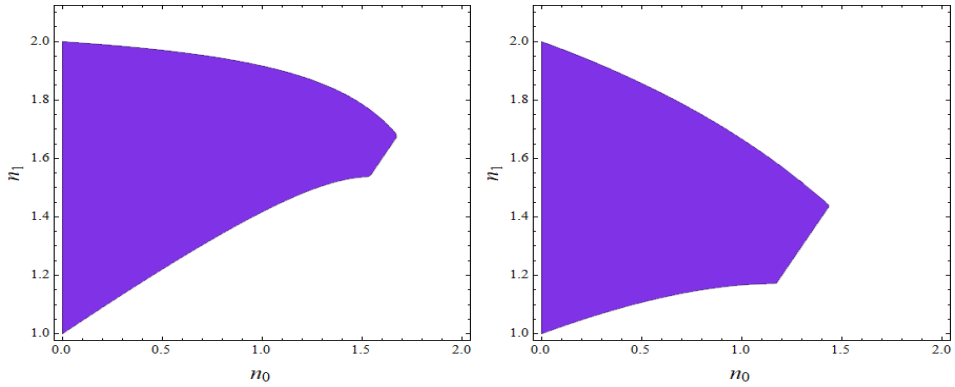

(a) $n_2 = 2.25$ (b) $n_2 = 4$

Figure 3: Constant n_2 slices of parameter space. The shaded regions are parameters values where an equilibrium solution exists.

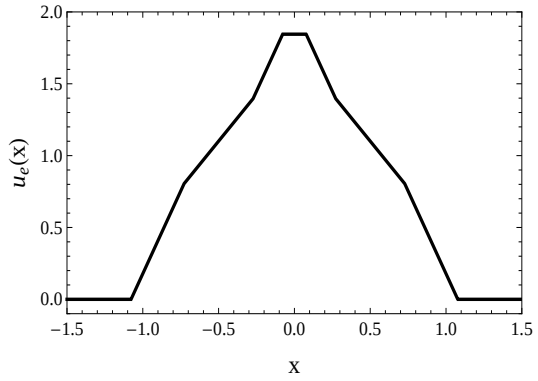

Figure 4: The equilibrium solution with parameter values $(n_0, n_1, n_2) = (1.3, 1.5, 2.3)$

2.2 Gaussian dispersal kernel

We consider the case where $k(x)$ is the Gaussian kernel. This is consistent with the biological assumption of a random diffusion process with a fixed stopping time. Since, as with the uniform case, scaling does not effect the existence/non-existence of equilibria for a given set of parameters, we choose to set the variance to $\frac{1}{12}$ to match the variance and proximately the length scale of the uniform case. With this choice, $k(x) = \sqrt{\frac{6}{\pi}}\, e^{-6x^2}$.

With this definition of $k(x)$, equation (5) becomes

$$
\begin{aligned}
A(a,b) &= -n_1 + \frac{(n_0 - n_2)}{2} \operatorname{erf}\left(2\sqrt{6}a\right) + \frac{n_2}{2}\left(\operatorname{erf}\left(\sqrt{6}(a+b)\right) + \operatorname{erf}\left(\sqrt{6}(b-a)\right)\right), \\
B(a,b) &= -1 + \frac{n_2}{2} \operatorname{erf}\left(2\sqrt{6}b\right) + \frac{(n_2 - n_0)}{2}\left(\operatorname{erf}\left(\sqrt{6}(b-a)\right) - \operatorname{erf}\left(\sqrt{6}(b+a)\right)\right), \\
C(a,b) &= -n_1 + (n_0 - n_2) \operatorname{erf}\left(\sqrt{6}a\right) + n_2 \operatorname{erf}\left(\sqrt{6}b\right),
\end{aligned}
\tag{7}
$$

with $\text{erf}(x) = \int_0^x \frac{2}{\sqrt{\pi}} e^{-s^2} \mathrm{d}s$.

With the definitions of A, B, and C given in equation (7), it is difficult to develop analytic conditions to determine when the algebraic system given in Theorem 2.1 has solutions for a given set of parameters. We instead rely on numerical methods to make this determination. Depending on how often the curves $A(a,b) = 0, B(a,b) = 0$ intersect in the region of the (a,b) plane where $C(a,b) > 0$, we find that there are parameter values for which there are 0,1, or 2 distinct (a,b) satisfying Theorem 2.1. This is illustrated in Figure 5. In the case of sub-figure (c), the two distinct solutions, correspond to two distinct equilibria for that set of parameters. In Figure 5 we use coordinates $(b-a, b+a)$ for the purpose of allowing better visualization of the intersection(s) of the curves.

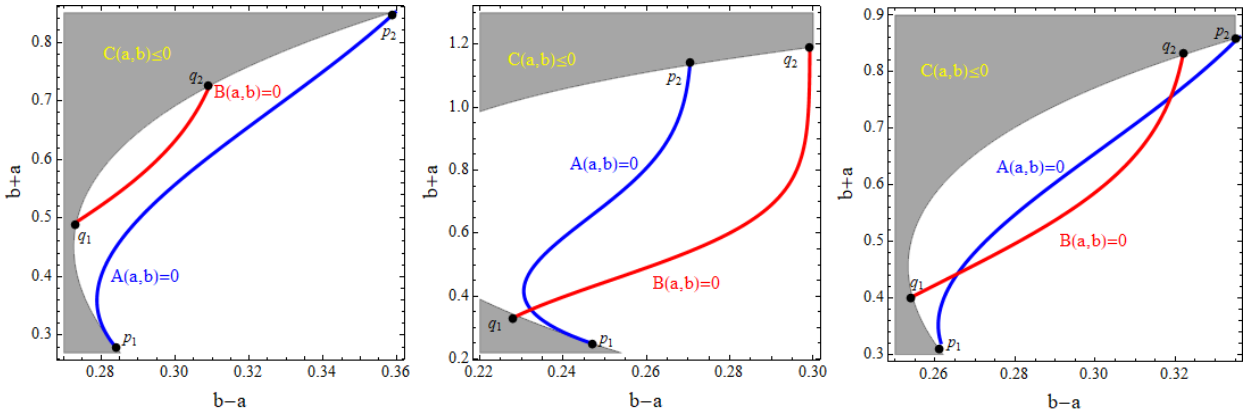

(a) $n_0 = 1.2, n_1 = 1.55, n_2 = 2.3$ (b) $n_0 = 1.3, n_1 = 1.4, n_2 = 2.3$ (c) $n_0 = 1.15, n_1 = 1.48, n_2 = 2.3$

Figure 5: Sub-Figure (a) illustrates a set of parameters having no solution to the algebraic system in Theorem 2.1, and thus no equilibria. Sub-Figure (b) illustrates a set of parameters having a single solution, and thus a single equilibrium. In sub-figure (c) we see a set of parameters where there are two distinct equilibria.

Similar to the case of the uniform kernel, we find that parameter values with two distinct equilibria and those with a single equilibria, both occupy a set of full measure in the parameter space $\{(n_0,n_1,n_2) \in \mathbb{R}^3 | n_0 < n_1 < n_2 \text{ and } n_1, n_2 > 1\}$. In Figure 6 we delineate the regions with single and double equilibria. To make the region plot in Figure 6, we developed an algorithm that takes (n_0,n_1,n_2) as an input and returns the number of equilibria for those parameter values. The algorithm first determines where the $A = 0$ and $B = 0$ curves intersect the $C = 0$ curve, these are the points labeled p_1, p_2, q_1, q_2 in Figure 5. In Figure 5,(a) and (c) we see q_1 and q_2 are nested between p_1 and p_2 along the $C = 0$ curve. By the continuity of the $A = 0, B = 0$ curves, with this condition it is only possible to have either zero-points where $A = 0$ intersects $B = 0$, as in sub-figure (a), or to have two-points where $A = 0$ intersects $B = 0$, as in sub-figure (c). If this condition is detected, the algorithm performs constrained numerical minimization of $A^2 + B^2$ with $C > 0$. If the minimum of $A^2 + B^2$ is less the 10^{-6} the algorithm returns 2, as it is not possible to have only one intersection in this case. If the minimum is greater then 10^{-6} then the algorithm returns 0. If the algorithm determines only single q lies between p_1 and p_2 on the $c = 0$ curve, such as in sub-figure (b), then the only possibility is that $A = 0$ and $B = 0$ have only 1 intersection in the $C > 0$ region, so the algorithm returns 1.

In Figure 7 typical equilibria for the gaussian kernel are depicted. In sub-figure (a), the parameter values have a single unique equilibrium. The value of a and b are 0.0626 and 0.2949 respectively. In sub-figure (b), there are two distinct equilibria. For the red equilibrium curve a and b are 0.0887 and 0.3543 respectively. For the blue equilibrium curve a and b are 0.2184 and 0.5372 respectively. These equilibria are positive on the whole real line.

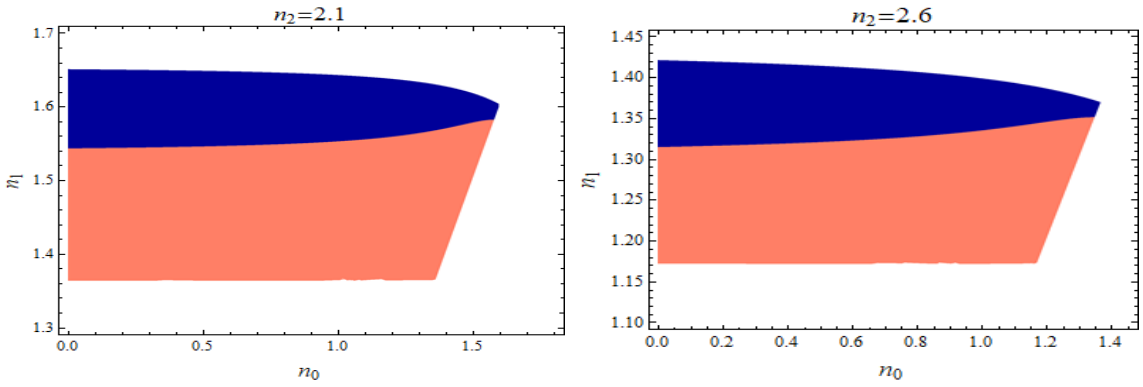

(a) (b)

Figure 6: Constant n_2 slices of parameter space. The salmon colored regions are parameter values with a single equilibrium. The blue regions are parameter values with 2 distinct equilibria.

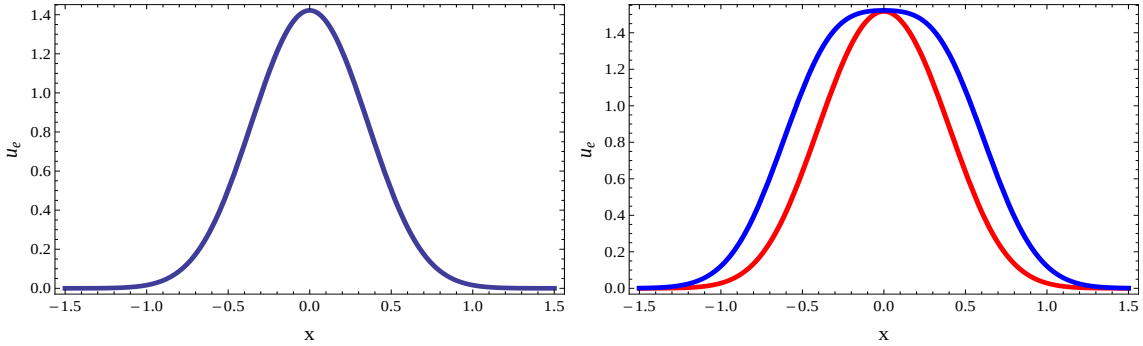

(a) $n_0 = 1.3, n_1 = 1.4, n_2 = 2.3$ (b) $n_0 = 1.15, n_1 = 1.48, n_2 = 2.3$

Figure 7: Typical equilibrium solutions for the Gaussian dispersal kernel. In sub-figure (a) the parameters have a single equilibrium. In sub-figure (b) the parameters have two distinct equilibria.

3 Numerical Results

3.1 Uniform dispersal with piecewise constant fecundity function

In Section 3.1 we demonstrated the existence of equilibrium solutions vanishing at $\pm\infty$ for the uniform kernel with the fecundity function defined in equation (3). In this section we will examine the behavior of perturbed equilibria. The iterates of model (1) are particularly easy to numerically compute for these definitions of k and g. If u_0 is a piecewise defined linear spline, then the intervals of x where $\{x\,|\,0 < u_0(x) < 1\}$, $\{x\,|\,1 < u_0(x) < n_1\}$, and $\{x\,|\,n_1 < u_0(x)\}$ can be determined, which in turn determines $g\big(u_0(x)\big)$. The convolution with $k(x)$ can then be exactly determined, thus giving $u_1(x)$.

To choose a parametric form of perturbation for u_e, equation (3) provides us a suggestive form. Namely by shifting the discontinuity points of $G_{\{a,b\}}$ from $\{-b, -a, a, b\}$ to the respectively nearby points $\{-b_1, -a_1, a_2, b_2\}$ and then taking the convolution with k, we can create a four parameter perturbed equilibrium that converges to u_e as $b_1, b_2 \to b$ and $a_1, a_2 \to a$. This form is fairly general, in that it represents the first iterate of any

uni-modal initial data that exceeds n_1 at its maximum.

We define the perturbed initial state as

$$\tilde{u}_e = k * \widetilde{G}_{\{-b_1,-a_1,a_2,b_2\}},$$

where

$$\widetilde{G}_{\{-b_1,-a_1,a_2,b_2\}}(x) = \begin{cases} n_2, & -b_1 < x < -a_1 \\ n_0, & -a_1 < x < a_2 \\ n_2, & a_2 < x < b_2 \\ 0, & \text{otherwise.} \end{cases} \tag{8}$$

Obviously the parameters must conform to the inequality $-b_1 < -a_1 < a_2 < b_2$, and so as to neglect trivial translations we choose $\{-b_1, -a_1, a_2, b_2\}$ so as to fix the center of mass of $\widetilde{G}_{\{-b_1,-a_1,a_2,b_2\}}(x)$ at $x = 0$.

To study the stability of the equilibriums it is helpful to use a domain-size versus time plot. For our purposes we define the domain size of $u_i(x)$ to be the length of the support of $u_i(x)$ in the case that the support is a single interval, or more generally as $\sup\{x\,|\,u_i(x) > 0\} - \inf\{x\,|\,u_i(x) > 0\}$. For instance, if the domain size is linearly increasing with time, this indicates the perturbed solution has converged to a spreading solution. If the domain size oscillates with a period p, this is a strong indication that the perturbed solution has converged to a period-p attractor.

We observe a wide variety of behaviors. For a fixed n_2, if weaker growth parameters are chosen for n_1 and n_0, then perturbations to the equilibrium can lead to extinction. This is observed in Figure 8. For a fixed n_2, if strong growth parameters are chosen for n_1 and n_0, then perturbations to the equilibrium can lead to spreading solutions, as is observed in Figure 9. However for intermediate values of n_1 and n_0 a wide variety of stable nonspreading periodic solutions can be found. For example in Figures 11-10, the same set of parameters can lead either to a nonspreading period-5 orbit, or a nonspreading period-105 orbit depending on the initial perturbation. A wide a variety of short and long periodicities can be observed for other parameter values.

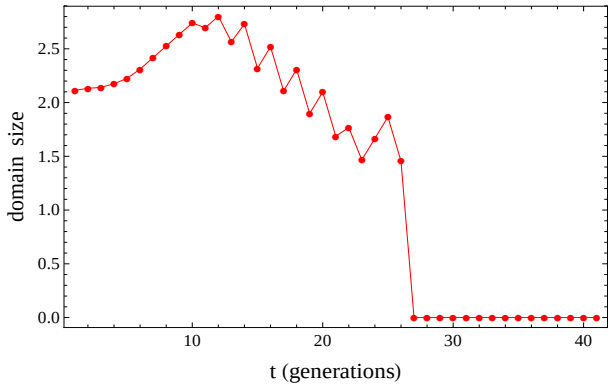

Figure 8: A domain-size vs. time plot of an equilibrium where perturbation leads to extinction. $\{n_0, n_1, n_2\} = \{1.1, 1.4, 2.5\}$. The equilibrium is $k * G_{\{0.2334,\,0.5548\}}$, and the perturbed initial state is $k * \widetilde{G}_{\{-0.5553,\,-0.2212,\,0.2353,\,0.5586\}}$.

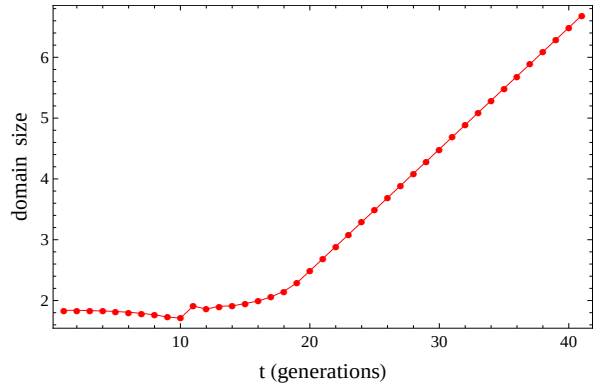

(a) domain-size vs. time

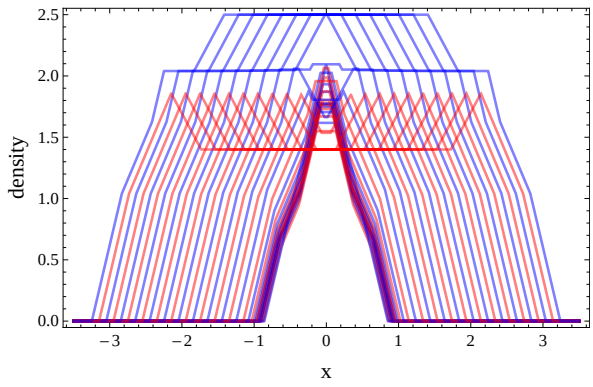

(b) Plot of $u_1(x)$ through $u_{40}(x)$ vs. x. Red denotes odd years, blue denotes even years.

Figure 9: A case where perturbations lead to spreading solutions. $\{n_0, n_1, n_2\} = \{1.4, 1.6, 2.5\}$. The equilibrium is $k * G_{\{0.1508,\, 0.4236\}}$, and the perturbed initial state is $k * \widetilde{G}_{\{-0.4189,\, -0.1439,\, 0.1471,\, 0.4193\}}$.

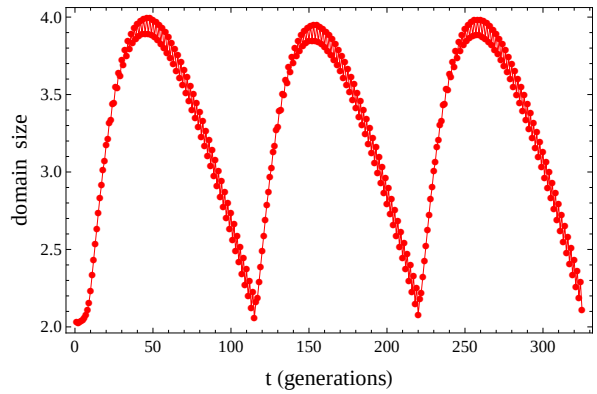

(a) domain-size vs. time

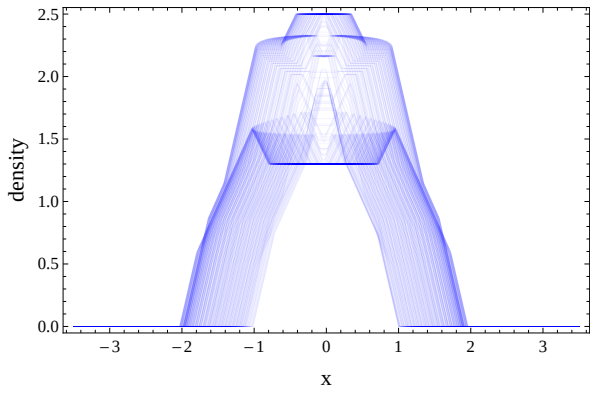

(b) Plot of $u_1(x)$ through $u_{325}(x)$. Curves are rendered partially transparent so as to show points of accumulation.

Figure 10: A case where the same parameters used in Figure 11 have a different orbit when a different initial condition is used. The periodicity of this orbit is 105. The initial state is $k * \widetilde{G}_{\{-0.5160,\, -0.2232,\, 0.2387,\, 0.5193\}}$.

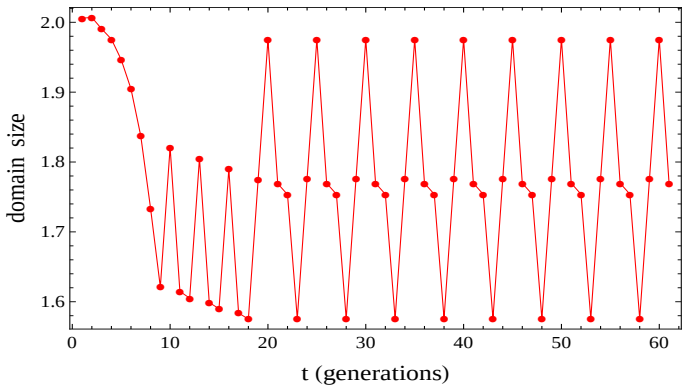

(a) domain-size vs. t

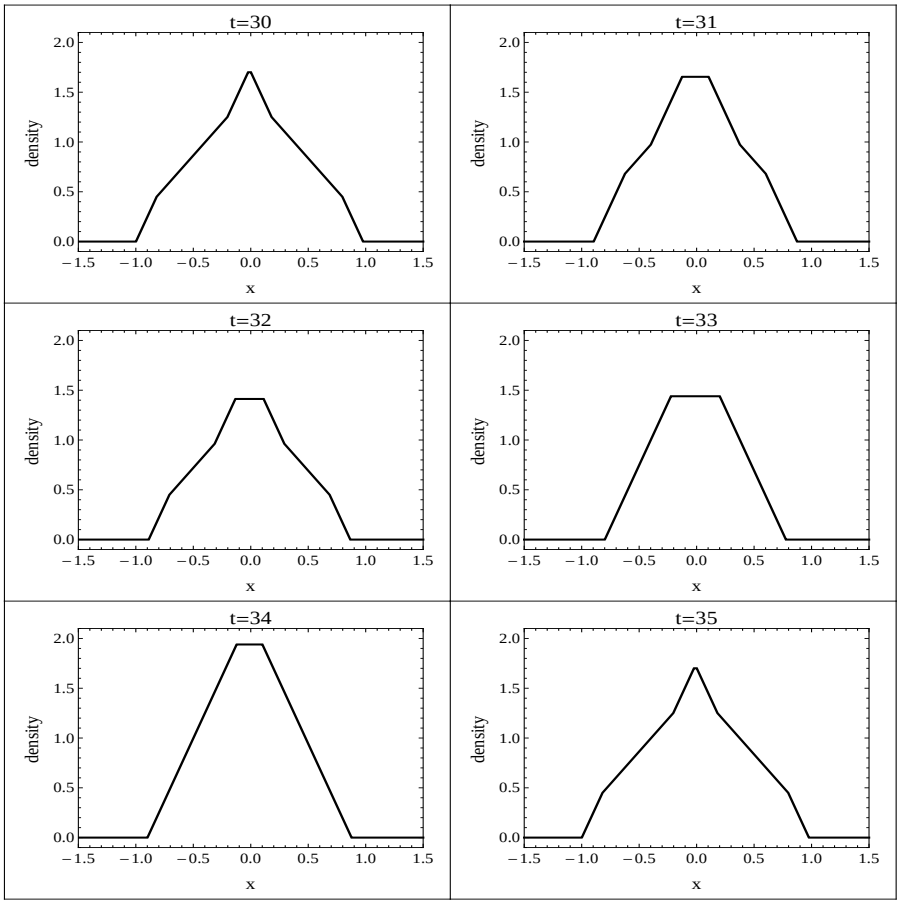

(b) sequence of density curves

Figure 11: A perturbation leading to a period-5 orbit. $\{n_0, n_1, n_2\} = \{1.3, 1.45, 2.5\}$. The equilibrium is $k * G_{\{0.2205,\, 0.5122\}}$, and the perturbed initial state is $k * \widetilde{G}_{\{-0.5024,\, -0.2078,\, 0.2134,\, 0.5035\}}$. Sub-figure (b) shows a plot of $u_{30}(x)$ through $u_{35}(x)$ showing a complete period.

3.2 Gaussian dispersal with piecewise constant fecundity function

In Section 3.2 we analytically demonstrated the existence of equilibrium solutions in the form $k * G_{\{a,b\}}$ when k is the Gaussian distribution. In this section we will examine the evolution of perturbed equilibria. As in Section 4.1, we will consider initial data in the form $k * \widetilde{G}_{\{-b_1,-a_1,a_2,b_2\}}$ where $\widetilde{G}$ is defined as in equation (8). Since the Gaussian distribution does not have compact support, we must define domain-size slightly differently then in Section 4.1. In this section we define the reference domain-size of $u_i(x)$ to be the length of the interval where $u_i(x) > 1$ in the uni-modal case, The threshold of $u_i(x) = 1$ is chosen as that corresponds to the Allee threshold. More generally we define the reference domain size to be $\sup\{x \,|\, u_i(x) > 1\} - \inf\{x \,|\, u_i(x) > 1\}$.

As with the uniform case, we see a wide variety of phenomena. We have found instances of perturbed solutions converging to period-2 orbits, period-4 orbits, irregular orbits, and extinction. For parameter values with 2 distinct equilibria (blue regions in Figure 6) we observe that the perturbed solutions converge to the same pattern of oscillation regardless of which perturbed equilibrium the solution was initiated with. We observe no distinction between the patterns of periodic oscillations that occur with the 1-equilibrium parameters versus the 2-equilibrium parameters. Stated slightly differently, for a given pattern of oscillation, instances of parameters exhibiting that type of oscillation can be found in both the blue and salmon regions of Figure 6. In contrast to the uniform-kernel case, we did not observe spreading solutions for small perturbations.

In Figure 12 a set of parameters with an attracting period-2 orbit is depicted. Both the equilibria, depicted by the dashed-curves in sub-Figure (b), when perturbed stabilize to the same period-2 pattern. In Figure 13 a case where a single equilibrium is attracted to a period-4 orbit is depicted. Finally in Figure 14 a set of parameters that develops an irregular, but nonspreading orbit is depicted. A high sensitivity to initial conditions is observed for the parameters in Figure 14, suggesting chaotic dynamics.

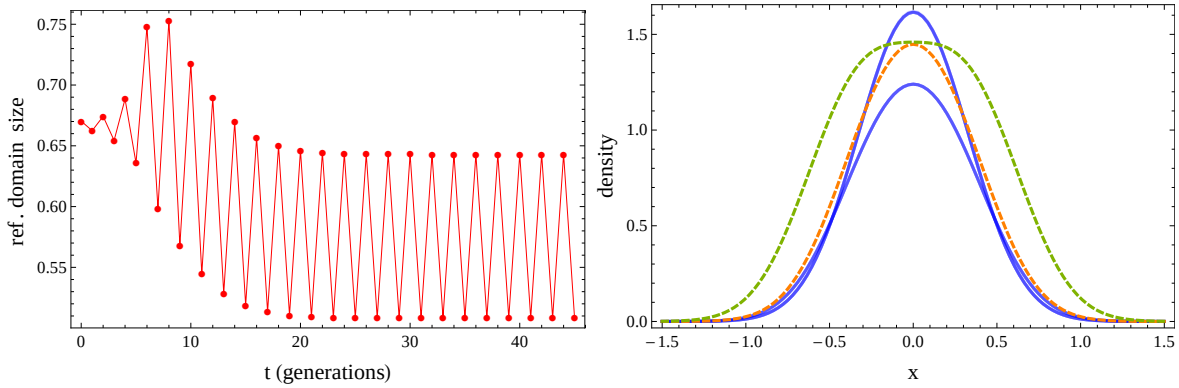

(a) Ref. domain-size vs. time.

(b) Plot of $u_{20}(x)$ through $u_{40}(x)$ vs. x. Equilibria are the dashed curves, period-2 curves are in blue.

Figure 12: A case where perturbations lead to period-2 oscillations. $\{n_0, n_1, n_2\} = \{1.25, 1.36, 2.6\}$. The equilibriums are $k * G_{\{0.1399,\, 0.3322\}}$ and $k * G_{\{0.3087,0.5279\}}$. The perturbed initial state used in this figure is $k * \widetilde{G}_{\{-0.3373,\, -0.1560,\, 0.1374,\, 0.3330\}}$.

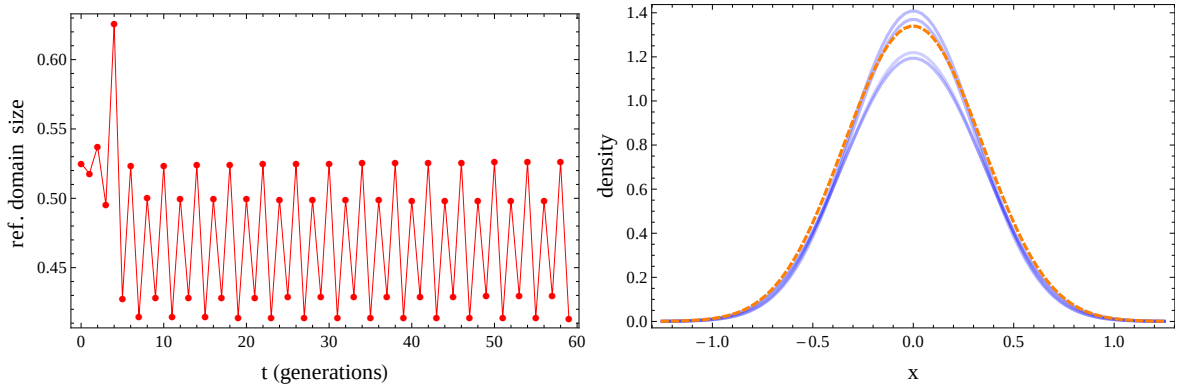

(a) ref. domain-size vs. time

(b) Plot of $u_{10}(x)$ through $u_{20}(x)$ vs. x, the single equilibrium is the dashed curve.

Figure 13: A case where perturbations lead to period-4 oscillations. $\{n_0, n_1, n_2\} = \{1.25, 1.3, 2.6\}$. The equilibrium is $k * G_{\{0.0849,\, 0.2618\}}$. The perturbed initial state used in the figure is $k * \widetilde{G}_{\{-0.2634,\, -0.0933,\, 0.0845,\, 0.2618\}}$.

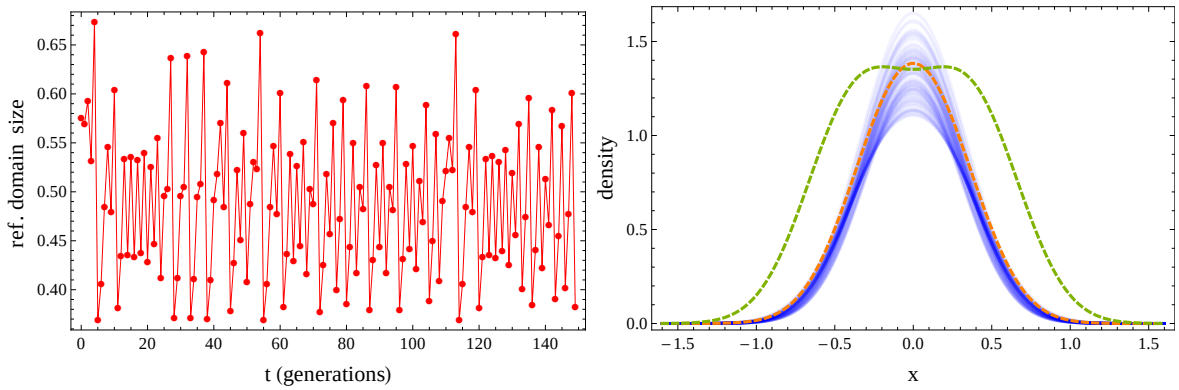

(a) ref. domain-size vs. time

(b) Plot of $u_{20}(x)$ through $u_{150}(x)$ vs. x, equilibriums are the dashed curves. The $u_i(x)$ (in blue) are rendered semi-transparent so as to show points of accumulation.

Figure 14: A case where perturbations lead to irregular oscillations. $\{n_0, n_1, n_2\} = \{1.05, 1.34, 2.6\}$. The equilibriums are $k * G_{\{0.0929,\, 0.2889\}}$ and $k * G_{\{0.3091, 0.5576\}}$. The perturbed initial state used in this figure is $k * \widetilde{G}_{\{-0.2866,\, -0.0884,\, 0.1011,\, 0.2891\}}$.

3.3 Numerical results for other growth functions

Thus far our results have focused on nonspreading solutions involving the piecewise constant growth function described in Eq. 2. To demonstrate that nonspreading solutions can occur for more general growth functions, we conduct numerical simulations for several variants of the Ricker growth function. Using the example of Schreiber (2003) we consider a growth function of the form $g(u) = u \exp\big(r(1-u)\big) I(u)$, where the positive density dependance at low densities (i.e. Allee effect) is encapsulated in $I(u)$. While Schreiber specifically examines a case where $I(u)$ is a Hill function with exponent 1, we will consider the more general case where $I(u)$ is any Hill function. Throughout this section we use the exponential power distribution $k(x) =$

$1.1109 \exp\left(-\left(\frac{x}{0.4965}\right)^4\right)$, whose variance is $\frac{1}{12}$ in keeping with the previous cases, and whose kurtosis is intermediate to that of the Gaussian and Uniform distributions of the same variance. Throughout, we also use Heaviside Pi (boxcar function) initial data of half-width 0.5 and height 1.25.

3.3.1 Truncated-Ricker function with linear strong-Allee effect

Thus far we have only considered growth functions with a rather severe form of strong Allee effect where $g(u)$ is zero on $[0,1)$. To demonstrate that nonspreading solutions can occur even for linear strong Allee effect, we consider the following growth function:

$$g(u) = \begin{cases} \rho\, u, & u < 1 \\ u \exp\left(1.35(1.5-u)\right), & u > 1. \end{cases} \tag{9}$$

We find that for $0 \leq \rho \leq 0.55$ there are asymptotically stable equilibrium solutions. The solutions for $\rho = 0.4$ are depicted in Figure 15. For $\rho > .55$ non-chaotic spreading solutions occur.

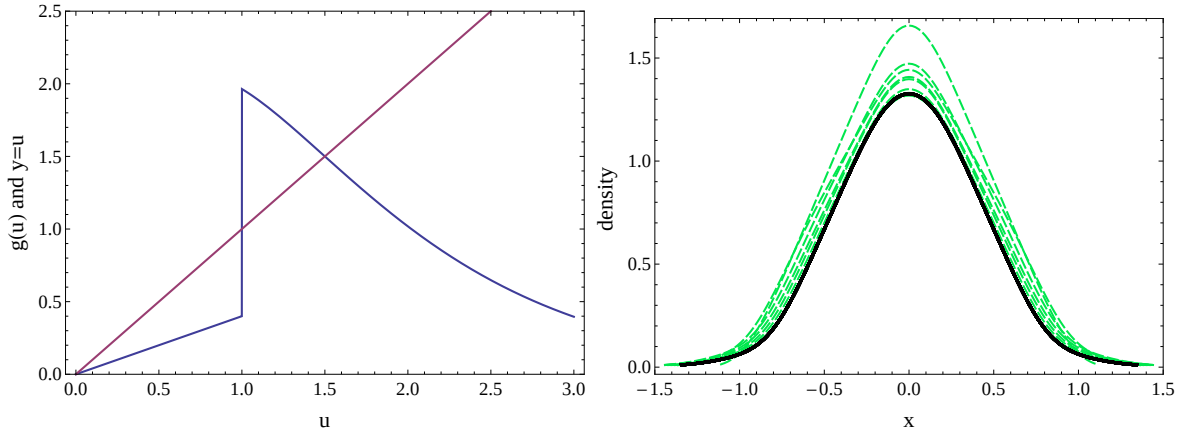

(a) $g(u)$ (b) $u_1(x)$ through $u_{80}(x)$

Figure 15: Plots of the growth function, transient iterations, and asymptotic attractor for the growth function in Eq. 9 with $\rho = 0.4$. In sub-figure (b)iterations 1-30 are shown in dashed-green, iterations 31-80 are shown in black.

It is worth noting that when $\rho = 0$ this becomes truncated Ricker function which was studied by Sullivan (2017) in terms of fluctuating invasion speeds for model (1). This can also be considered as a limiting case of the Hill-Ricker growth function, which we will discuss next, as the exponent tends to infinity. We find the results in this case to be similar to that depicted in Figure 15-(b).

3.3.2 Hill-Ricker function

We next consider

$$g(u) = u \exp\left(r(1-u)\right) \left(\frac{(1+1.3^7)\left(\frac{u}{1.3}\right)^7}{1+\left(\frac{u}{1.3}\right)^7} \right),$$

where we leave r as a bifurcation parameter. An example of this function with $r = 2.5$ is depicted in Figure 16-(a). For $r < 2.44$ (to 2 decimals) we find chaotic spreading solutions. For $2.44 < r < 2.64$ we find stable period 2 oscillations as depicted in Figure 16.

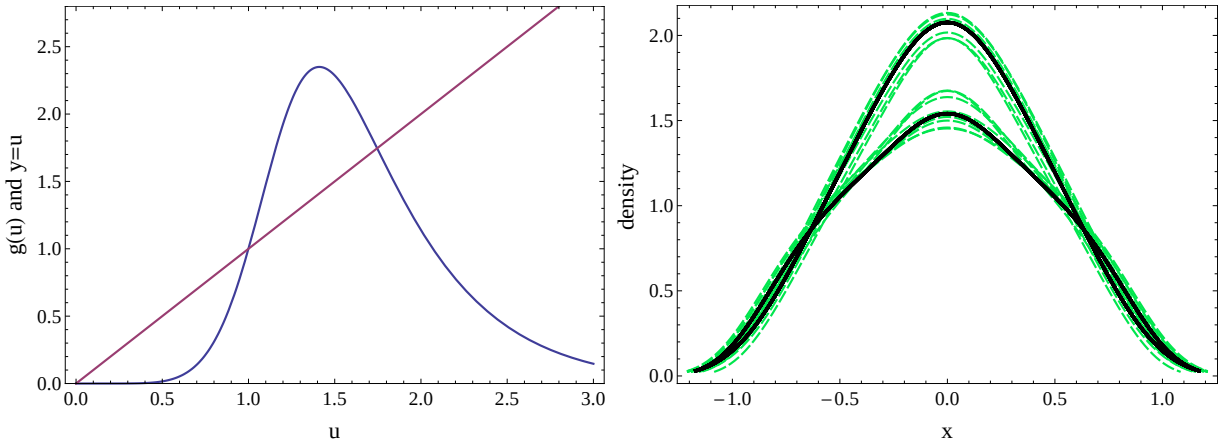

(a) $g(u)$ for Hill-Ricker function.

(b) $u_1(x)$ through $u_{80}(x)$.

Figure 16: Plots of the growth function, transient iterations, and attracting period-2 orbit for the Hill-Ricker function with $r = 2.5$. In sub-figure (a) we plot the Hill-Ricker growth function. In sub-figure (b) iterations 1-30 are shown in dashed-green, iterations 31-80 are shown in black.

For $2.64 < r < 2.91$ we find a asymptotically stable equilibriums as depicted in Figure 17. For $r > 2.91$ extinction occurs.

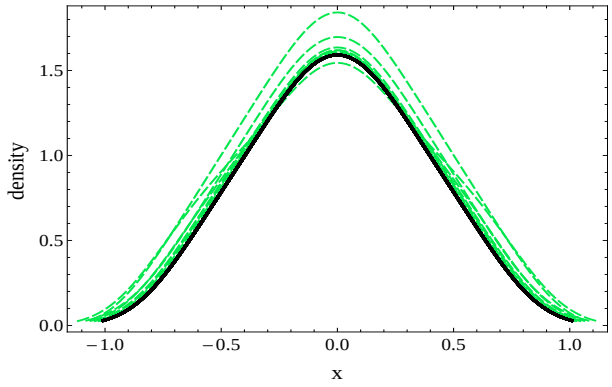

Figure 17: Plots of solution curves for $r = 2.8$ converging to a period-1 attractor. Iterations 1-30 are shown in dashed-green, iterations 31-80 are shown in black.

3.3.3 Hill-Ricker function with long initial data

Thus far in section 4.3 we have considered the evolution of the population with relatively simple initial data, namely a boxcar function whose support, $(-0.5, 0.5)$, is comparable in length scale to that of a typical nonspreading solution, such as in Figure 17. We now wish to consider the evolution when the support of the initial data is much larger then that of a single equilibrium solution. We will use the Hill-Ricker growth function with $r = 2.8$, which has a single asymptotically stable equilibrium solution (depicted in Figure 17).

Since the length scale of the equilibrium is roughly 2 length units, we will initiate over an interval of length much larger then 2, and let the density be super-Allee threshold with small fluctuations over length-scales of σ. To accomplish this we will use a piecewise constant function, constant over sub-intervals of length σ, whose height on each sub-interval is given by a random variate drawn from the uniform distribution on $(1.1, 1.2)$. The functional form is thus

$$u_0(x) = \begin{cases} 0\,, & |x| > n\sigma \\ u_{\{-n\}}\,, & -n\sigma < x < (-n+1)\sigma \\ u_{\{-n+1\}}\,, & (-n+1)\sigma < x < (-n+2)\sigma \\ \ddots & \ddots \\ u_{\{n-2\}}\,, & (n-2)\sigma < x < (n-1)\sigma \\ u_{\{n-1\}}\,, & (n-1)\sigma < x < n\sigma \end{cases}$$

where $u_{\{i\}}$ are independent identically distributed uniform $(1.1, 1.2)$ random variates.

We then consider cases where $\sigma >> 2$, $\sigma = 2$, and $\sigma << 2$ while holding the initial support to be $(-40, 40)$.

As can be seen in Figures 18-20, stable non-interacting patches emerge from the initial data after sufficient time. As can be seen in Figure 18, when the scale of variation in the initial data in long compared to the size of the equilibrium, stable patches are sparse and tend to occur only near places of relatively large fluctuations in the initial data such as near $x = -36, x = -30$ for instance. In Figure 19 with $\sigma = 2$ we see the density of stable patches is much higher then in the $\sigma = 6$ case with patch formations till tending to occur near places sharp jumps in initial density. In the case of small σ in Figure 20 we see the total patch formation density is not significantly different form that in Figure 19 suggesting saturation. The pattern of where stable patches will form is not readily discernable.

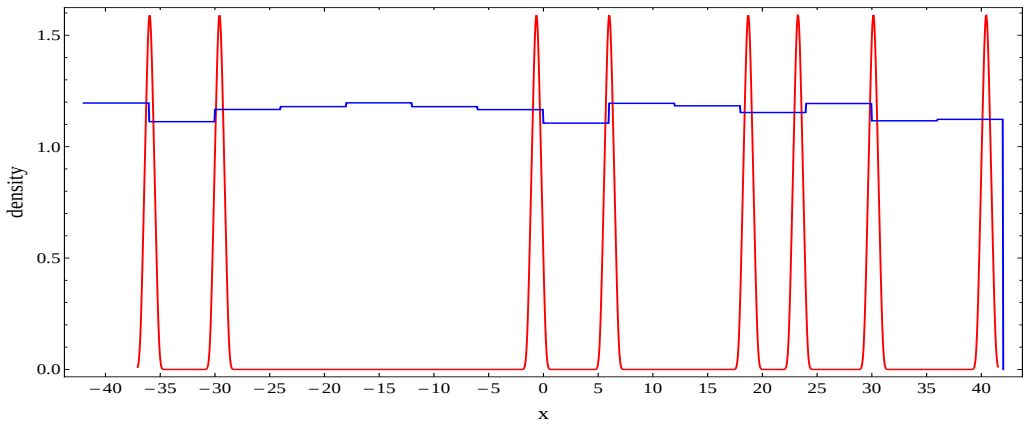

Figure 18: Pattern formation with $\sigma = 6$. Initial data is shown in blue, iterations $110 - 120$ are shown in red.

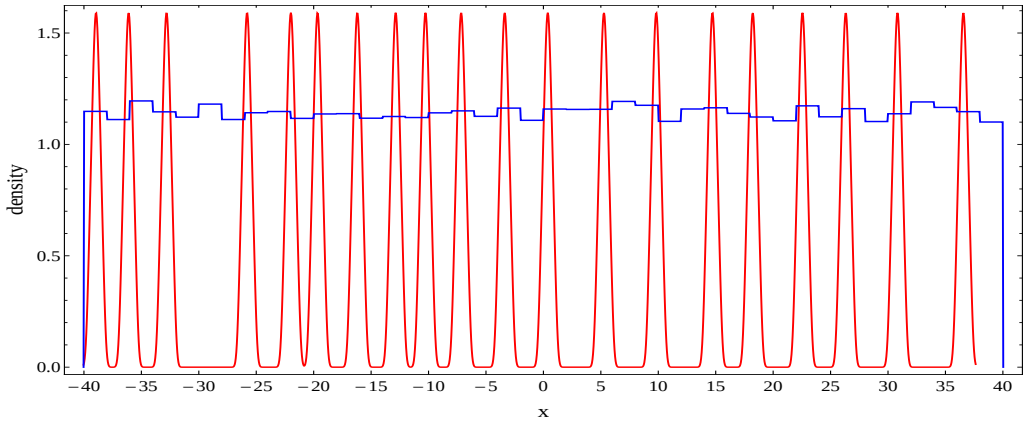

Figure 19: Pattern formation with $\sigma = 2$. Initial data is shown in blue, iterations $110 - 120$ are shown in red.

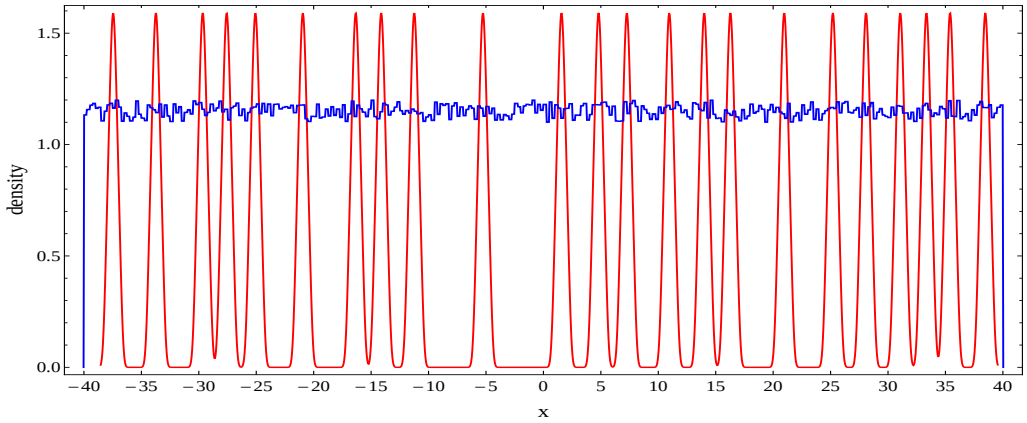

Figure 20: Pattern formation with $\sigma = 0.25$. Initial data is shown in blue, iterations $110 - 120$ are shown in red.

4 Discussion

In this paper we studied the spatial dynamics of model (1) with the growth function exhibiting both an Allee effect and overcompensation. We analytically studied the case that $g(u)$ is a piecewise constant function, and provided conditions for the existence of equilibrium solutions vanishing at $\pm\infty$. We tested the conditions for the uniform distribution kernel and Gaussian kernel. We found that for each of them there exists a solid region in the parameter space where there is an equilibrium solution, and for the Gaussian kernel there also exists a solid region where there are two distinct equilibrium solutions. We carried out numerical simulations for perturbations of the equilibrium solutions, and found that the model can generate nonspreading solutions with various spatial patterns. We also conducted simulations for the truncated Ricker function with linear strong Allee effect and for the Hill-Ricker function, and found that there are stable period-one and period-two equilibrium solutions with zero value at $\pm\infty$. Our results show a variety of interesting behaviors in model (1): attracting equilibrium solutions with different periods, nonspreading solutions with various periodicities in density and domain size, and nonspreading solutions with chaos in density and domain size, spreading solutions , and extinction.

The spatial dynamics of (1) depend on $g(u)$, $k(x)$, and the initial data. Let L denote the size of the interval over which the initial density is above the Allee threshold. Our simulations show that for $g(u)$ given by the piecewise constant growth function, and $k(x)$ given by the uniform distribution, (i) if L is 'small' then the solution will converge to zero, (ii) if L is 'medium' then the solution is nonspreading and it persists, and (iii) if L is 'large' then the solution spreads at a oscillatory speed in each direction. However for $g(u)$ given by the Hill-Ricker function and $k(x)$ given by the uniform distribution, an initial distribution with a large L can lead to patch formation where all the emerging static patches are basically translations of a stable equilibrium solution vanishing at $\pm\infty$.

Robust nonspreading solutions are now known to exist even in basic single-species integro-difference equations. This discovery demonstrates novel phenomena in biological invasions, and relates deeply to biological observations. It helps us understand important questions such as how populations spread across landscapes, and why populations are often patchily distributed in space. This paper represents the first attempt to establish robust nonspreading solutions in integro-difference equations. New important research topics include: (i) to establish existence of equilibrium solutions for a general growth function; (ii) to determine existence of traveling waves; (iii) to study stability of equilibrium solutions and traveling waves, and (iv) to explore patch formation. New techniques are needed to address (i). Two particular types of traveling waves are of interest. One type is about waves vanishing at both ∞ and $-\infty$, and the other one is about waves vanishing at ∞ and above a positive number near $-\infty$. The analysis for existence of equilibrium solutions will be useful for establishing traveling waves, as an equilibrium solution is also a traveling wave. The spectral stability methods in [33, 41, 42] are useful for studying stability of traveling waves. To explore pattern formation, one approach is to first investigate how two equilibrium solutions with one being a translation of the other interact to develop new spatial patterns. We leave these problems for future investigation.

5 Appendix

5.1 Appendix A, Proof of Theorem 2.1

Suppose there exists an a, b such that $0 < a < b$ and

$$A(a,b) = 0,\ B(a,b) = 0,\ C(a,b) > 0.$$

Letting $u_1(x) = \big(k * G_{\{a,b\}}\big)(x)$, it then follows from the definition of A, B, C in equation (5) that $u_1(0) > n_1$, $u_1(a) = n_1, u_1(b) = 1$. Therefore if

1. for all $x \in (-a,a),\ u_1(x) > n_1$,
2. for all $x \in (-b,-a) \cup (a,b),\ 1 < u_1(x) < n_1$,
3. for all $|x| > b,\ u_1(x) < 1$,

it then follows by the definition of g in equation (2) that $g(u_1(x)) = G_{\{a,b\}}(x)$. We therefore see that $Q[u_1] = \big(k * g(u_1)\big) = \big(k * G_{\{a,b\}}\big) = u_1$ and therefore u_1 is an equilibrium of model (1).

5.2 Appendix B

We wish to derive the conditions on n_0, n_1, n_2 where the conditions in Theorem 2.1 will be satisfied for the uniform dispersal kernel. We first note that in equations A, B, C (from equation (5)), a and b only appear in

the arguments of K in the form $a+b, 2b, 2a, b-a, b, a$.

Since $a+b, 2b, 2a, b-a, b, a$ are all positive and K is piecewise defined as

$$K(x) = \begin{cases} 0, & x < \frac{-1}{2} \\ \frac{1}{2}+x, & \frac{-1}{2} \leq x \leq \frac{1}{2} \\ 1, & x > \frac{1}{2}, \end{cases}$$

we see it is necessary to make assumptions about if $a+b, 2b, 2a, b-a, b, a$ are less then or greater then $\frac{1}{2}$ to determine which sub-function of K is applicable in equation (5). In Figure 21 the different colored regions correspond to different values for the Boolean valued vector $\{a+b > \frac{1}{2}, 2b > \frac{1}{2}, 2a > \frac{1}{2}, b-a > \frac{1}{2}, b > \frac{1}{2}, a > \frac{1}{2}\}$.

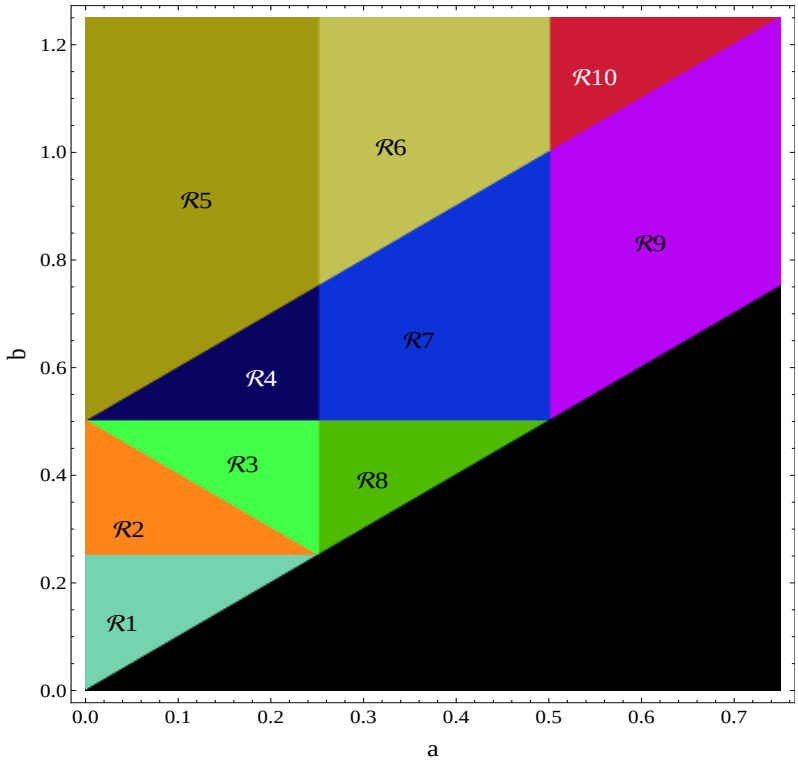

Figure 21: Regions of the (a,b) plane where the Boolean vector $\{a+b > \frac{1}{2}, 2b > \frac{1}{2}, 2a > \frac{1}{2}, b-a > \frac{1}{2}, b > \frac{1}{2}, a > \frac{1}{2}\}$ takes distinct values.

For each region we make the appropriate substitution for the sub-functions of $K(\cdot)$ and attempt to solve the system $A(a,b) = 0, B(a,b) = 0$. We find that for regions $\mathscr{R}_1, \mathscr{R}_5, \mathscr{R}_6, \mathscr{R}_7, \mathscr{R}_8, \mathscr{R}_9, \mathscr{R}_{10}$ the resulting system, which is linear in a, b, has a zero determinant, and thus generally no solutions.

For region $\mathscr{R}_2$ the resulting system $A(a,b) = 0, B(a,b) = 0$ becomes

$$2(n_2 - n_0)a - 2n_2 b = -n_1,$$

$$4(n_2 - n_0)a = n_2 - 2.$$

The solution to this system is

$$a = \frac{n_2 - 2}{4(n_2 - n_0)}, \; b = \frac{n_2 + 2n_1 - 2}{4n_2}.$$

However when this result is substituted into $C(a,b)$ with the appropriate assumptions, it is found $C(a,b) = 0$ thus violating the hypothesis of Theorem 2.1 and there are not any valid equilibria.

For region $\mathscr{R}_3$ and $\mathscr{R}_4$ the resulting system for $A(a,b) = 0, B(a,b) = 0$ becomes

$$(2n_0 - 3n_2)a + n_2 b = -\frac{n_2}{2} + n_1$$

$$(n_0 - n_2)a + (n_2 - n_0)b = 1 - \frac{n_0}{2}.$$

The unique solution to the system, which we use to define the functions $\hat{a}(n_0,n_1,n_2), \hat{b}(n_0,n_1,n_2)$ is given by

$$a = \hat{a}(n_0,n_1,n_2) := \frac{2n_0(n_1 - n_2) + n_2(2 - 2n_1 + n_2)}{4(n_2 - n_0)^2}$$

$$b = \hat{b}(n_0,n_1,n_2) := \frac{2n_0^2 + n_2(6 - 2n_1 + n_2) + 2n_0(n_1 - 2n_2 - 2)}{4(n_2 - n_0)^2}.$$

When $C(a,b)$ is evaluated at $\left(\hat{a}(n_0,n_1,n_2), \hat{b}(n_0,n_1,n_2)\right)$ and simplified with the assumption that

$$\left(\hat{a}(n_0,n_1,n_2), \hat{b}(n_0,n_1,n_2)\right) \in \mathscr{R}_3 \cup \mathscr{R}_4$$

it is found $C(\hat{a},\hat{b}) > 0$. Thus the characterization for the existence of equilibriums with the uniform kernel becomes: There exists an equilibrium if $\left(\hat{a}(n_0,n_1,n_2), \hat{b}(n_0,n_1,n_2)\right) \in \mathscr{R}_3 \cup \mathscr{R}_4$.

References

[1] W. C. Allee. 1931. Animal Aggregations. A Study on General Sociology. University of Chicago Press, Chicago, IL.

[2] W. C. Allee, A. E. Emerson, O. Park, T. Park, and K. P. Schmidt. 1949. Principles of Animal Ecology, W. B. Saunders, Philadelphia, Pennsylvania, USA.

[3] T.-L. Ashman, T. M. Knight, J. A. Steets, P. Amarasekare, M. Burd, D. R. Campbell, M. R. Dudash, M. O. Johnston, S. J. Mazer, R. J. Mitchell, M. T. Morgan, and W. G. Wilson. 2004. Pollen limitation of plant reproduction: ecological and evolutionary causes and consequences. Ecology **85**: 2408-2421.

[4] M. Burd. 1994. Bateman's principle and plant reproduction-the role of pollen limitation in fruit and seed set. Bot. Rev. **60**: 83-139.

[5] S. L. Cadre, T. Tully, S. J. Mazer, J.-B. Ferdy, J. Moret, and N. Machon. 2008. Allee effects within small populations of Aconitum napellus ssp. lusitanicum, a protected subspecies in northern France. New Phytologist **179**: 1171-1182.

[6] J. M. Calabrese and W. F. Fagan. 2004. Lost in time, lonely, and single: reproductive asynchrony and the Allee effect. American Naturalist **164**: 25-37.

[7] H. Caswell, M. G. Neubert, and C. M. Hunter. 2011. Demography and dispersal: Invasion speeds and sensitivity analysis in periodic and stochastic environments. Theor. Ecol. **4**: 407-421.

[8] H. Chen. 2014. A spatiotemporal pattern analysis of historical mountain pine beetle outbreaks in British Columbia, Canada. Ecography **37**: 344-356.

[9] F. Courchamp, L. Berec, and J. Gascoigne. 2008. Allee Effects in Ecology and Conservation. Oxford University Press, London.

[10] F. Courchamp, T. Clutton-Brock, and B. Grenfell. 1999. Inverse density dependence and the Allee effect, Trends in Ecology and Evolution **14**: 405-410.

[11] H. G. Davis, C. M. Taylor, J. G. Lambrinos, and D. R. Strong. 2004. Pollen limitation causes an Allee effect in a wind-pollinated invasive grass (Spartina alterniflora). Proc. Natl. Acad. Sci. USA. **101**: 13804-13807.

[12] B. Dennis. 1989. Allee effects: population growth, critical density, and the chance of extinction. Natural Resource Modeling **3**: 481-537.

[13] M. J. Groom. 1998. Allee effects limit population viability of an annual plant. The American Naturalist **151**: 487-496.

[14] D. P. Hardin, P. Takáč, and G. F. Webb. 1988. Asymptotic properties of a continuous-space discrete-time population model in a random environment. Bull. Math. Biol. **26**: 361-374.

[15] D. P. Hardin, P. Takáč, and G. F. Webb. 1988. A comparison of dispersal strategies for survival of spatially heterogeneous populations. SIAM J. Appl. Math. **48**: 1396-1423.

[16] D. P. Hardin, P. Takáč, and G. F. Webb. 1990. Dispersion population models discrete in time and continuous in space. J. Math. Biol. **28**: 1-20.

[17] A. Hastings and K. Higgins. 1994. Persistence of transients in spatially structured ecological models. Science **263**: 1133-1136.

[18] S.-B. Hsu and X.-Q. Zhao. 2008. Spreading speeds and traveling waves for nonmonotone integrodifference equations. SIAM J. Math. Anal. 40: 776–789

[19] D. M. Johnson, A. M. Liebhold, P. C. Tobin, O. N. Bjørnstad. 2006. Allee effects and pulsed invasion by the gypsy moth. Nature **444**: 361-363.

[20] T. H. Keitt, M. A. Lewis, and R. D. Holt. 2001. Allee effects, invasion pinning, and species' borders. Am Nat. **157**: 203-216.

[21] M. Kot and W. M. Schaffer. 1986. Discrete-time growth-dispersal models. Math. Biosci. **80**: 109-136.

[22] M. Kot. 1989. Diffusion-driven period doubling bifurcations. Biosystems **22**: 279-287.

[23] M. Kot. 1992. Discrete-time traveling waves: Ecological examples. J. Math. Biol. **30**: 413-436.

[24] M. Kot, M. A. Lewis, and P. van den Driessche. 1996. Dispersal data and the spread of invading organisms. Ecology **77**: 2027-2042.

[25] M. Kot, J. Medlock, T. Reluga, and D. B. Walton. 2004. Stochasticity, invasions, and branching random walks. Theor. Popul. Biol. **66**: 175-184.

[26] B. Li, M. A. Lewis, and H. F. Weinberger. 2009. Existence of traveling waves for integral recursions with nonmonotone growth functions. J. Math. Biol. **58**: 323-338.

[27] M. Kot. 2001. Elements of Mathematical Ecology. Cambridge University Press. Cambridge, United Kingdom.

[28] B. M. H. Larson and S. C. H. Barrett. 2000. A comparative analysis of pollen limitation in flowering plants. Biol. J. Linn. Soc. **69**: 503-520.

[29] R. Lui. 1982. A nonlinear integral operator arising from a model in population genetics. I. Monotone initial data. SIAM. J. Math. Anal. **13**: 913-937.

[30] R. Lui. 1982. A nonlinear integral operator arising from a model in population genetics. II. Initial data with compact support. SIAM. J. Math. Anal. **13**: 938-953.

[31] R. Lui. 1983. Existence and stability of traveling wave solutions of a nonlinear integral operator. J. Math. Biol. **16**:199-220.

[32] B. A. Melbourne and A. Hastings. 2009. Highly variable spread rates in replicated biological

[33] J. R. Miller and H. Zeng. 2011. Stability of traveling waves for systems of nonlinear integral recursions in spatial population biology. Disc. Cont. Dyn. Sys. B. **16**: 895-925.

[34] D. A. Moeller. 2004. Facilitative interactions among plants via shared pollinators. Ecology **85**: 3289-3301.

[35] M. Neubert, M. Kot, and M. A. Lewis. 1995. Dispersal and pattern formation in a discrete-time predator-prey model. Theor. Pop. Biol. **48** : 7-43.

[36] M. G. Neubert, M. Kot, and M. A. Lewis. 2000. Invasion speeds in fluctuating environments. Proc. R. Soc. Lond. B. Biol. Sci. **267**: 1603-1610.

[37] B. M. Ochocki and T. E. X. Miller. 2017. Rapid evolution of dispersal ability makes biological invasions faster and more variable. Nat Commun. **8**: 14315.

[38] G. Otto. 2017. Non-spreading Solutiona in a Integro-Difference Model Incorporating Allee and Over-compensation Effects. Ph. D thesis, University of Louisville.

[39] E. Pachepsky and J. M. Levine. 2011. Density dependence slows invader spread in fragmented landscapes. Am. Nat. **177**: 18-28.

[40] I. M. Parker. 2004. Mating patterns and rates of biological invasion Proc. Natl. Acad. Sci. USA. **101**: 13695-13696.

[41] B. Sandstede. 2002. Stability of Travelling Waves.In: Handbook of Dynamical Systems (Edited by B Fiedler). Elsevier 983-1055.

[42] D. Sattinger. 1976. On the stability of waves of nonlinear parabolic systems. Advances in Math. **22**: 312-355.

[43] S. J. Schreiber and M. E. Ryan. 2011. Invasion speeds for structured populations in fluctuating environments. Theor. Ecol. **4**: 423-434.

[44] W. Shen. 2004. Traveling waves in diffusive random media. J. Dyn. Diff. Equ. **16**: 1011- 1060.

[45] N. Shigesada, K. Kawasaki, and E. Teramoto. 1986. Traveling periodic waves in hetergeneous environments. Theor. Popul. Biol. **30**: 143-160.

[46] B. W. Silvermann. 1986. Density Estimation for Statistics and Data Analysis. Chapman and Hall, New York.

[47] M. Slatkin. 1973. Gene flow and selection in a cline. Genetice **75**: 733-756.

[48] T. R. E. Southwood. 1978. Ecological Methods: with Particular Reference to The Study of Insect Populations. Chapman and Hall, London, UK.

[49] P. A. Stephens and W. J. Sutherland. 1999. Consequences of the Allee effect for behavior, ecology and conservation. Trends in Ecology and Evolution **14**: 401-405.

[50] L. L. Sullivan, B. Li, T. E. X. Miller, M. G. Neubert, and A. K. Shaw. 2017. Density dependence in demography and dispersal generates fluctuating invasion speeds. Proc. Natl. Acad. Sci. USA **114**: 5053-5058.

[51] M. E. Tarter and M. D. Lock. 1993. Model-Free Curve Estimation. Chapman and Hall, New York.

[52] J. A. Walter, D. M. Johnson, P. C. Tobin and K. J. Haynes. 2015. Population cycles produce periodic range boundary pulses. Ecography (Cop.) **38**: 1200-1211.

[53] M. H. Wang, M. Kot, and M. G. Neubert. 2002. Integrodifference equations, Allee effects, and invasions. J. Math. Biol. **44**: 150-168.

[54] H. F. Weinberger. 1978. Asymptotic behavior of a model in population genetics, in Nonlinear Partial Differential Equations and Applications, ed. J. M. Chadam. Lecture Notes in Mathematics **648**: 47-96. Springer-Verlag, Berlin.

[55] H. F. Weinberger. 1982. Long-time beahvior of a class of biological models. SIAM. J. Math. Anal. **13**: 353-396.

[56] H. F. Weinberger. 2002. On spreading speeds and traveling waves for growth and migration models in a periodic habitat. J. Math. Biol. **45**: 511-548.

[57] H. F. Weinberger, K. Kawasaki, and N. Shigesada. 2008. Spreading speeds of spatially periodic integrodifference models for populations with nonmonotone recruitment functions. J. Math. Biol. **57**: 387-411.

[58] C. Weiss-Lehman, R. A. Hufbauer and B. A. Melbourne. 2017. Rapid trait evolution drives increased speed and variance in experimental range expansions. Nat. Commun. **8**: 14303.

[59] J. L. Williams, B. E. Kendall and J. M. Levine. 2016. Rapid evolution accelerates plant population spread in fragmented experimental landscapes. Science **353**: 482-485.